Implementation of the variation-after-projection approach in calculations with a time-odd Hartree-Fock mean field

Tu Ya,[1,*] Yan He,[1,2] Zao-Chun Gao,[2,3,†] Jia-Qi Wang,[2] and Y. S. Chen[2]

[1]*School of Physics Science and Technology, Shenyang Normal University, Shenyang, People's Republic of China*
[2]*China Institute of Atomic Energy, Beijing 102413, People's Republic of China*
[3]*State Key Laboratory of Theoretical Physics, Institute of Theoretical Physics, Chinese Academy of Sciences, Beijing 100190, People's Republic of China*

We have implemented a new variation-after-projection (VAP) calculation based on a time-odd Hartree-Fock (HF) mean field. The exact Hessian matrix of the projected energy has been successively evaluated for the first time, which makes the VAP calculation much more stable. With the time-odd mean field, the present VAP can be applied to the yrast states not only in the even-even nuclei, but also in the odd-*A* and odd-odd ones. The VAP energies throughout all spins for some calculated *sd*-shell nuclei are very close to the corresponding shell model ones. Our calculations clearly show that the spin projection is very important in achieving a good approximation to the full shell model.

I. INTRODUCTION

Theoretically, wave functions for nuclear many-body quantum systems should be obtained by solving Schrödinger's equation. This is done in the full shell model (SM) calculations. However, full SM calculations up to now have been restricted to rather small model spaces due to the the combinatorial computational cost. To tackle the problem of the eigensystems in even larger model spaces, approximated methods, such as stochastic quantum Monte Carlo approaches [1,2] and shell model truncation [3] have been developed.

Beside those approximated methods, one can also use the variational techniques on the basis of one or more symmetry projected Hartree-Fock-Bogoliubov (HFB) vacuum states. Such techniques have been done in the VAMPIR method [4] and in our previous variation after projection (VAP) [5]. Among the VAMPIR approaches, the best results with one single HFB vacuum state are from the most general one, called as GCV (general complex VAMPIR), where the HFB transformation is completely unrestricted. However, GCV requires fivefold integration for the projections of the neutron number, proton number, and the spin, which is much too time consuming. On the other hand, in Ref. [5], we have shown that the spin projection is much more important than the isospin projection and the mass number projection. So, a simpler VAP can be the one that the HF mean field is taken and only the spin projection is performed. This requires only threefold integration, yet such VAP energies for the ground states in *sd*-shell nuclei are already within 1.5 MeV above the shell model ones [5] (also see Fig. 4 below).

However in Ref. [5], we imposed the time-reversal symmetry for the HF and HFB vacuum states. This restricts our VAP calculations only to the even spin yrast states in even-even nuclei. To describe the yrast states in odd-*A* and odd-odd nuclei as well as the even-even ones in a uniformed way, the time reversal symmetry breaking should be considered in the VAP calculations.

Moreover, in our practical calculations, we realized that the real HF transformation may not be enough even if we consider the time reversal symmetry breaking. For instance, with real HF mean field, we cannot obtain a stable 1^+ state in an even-even nucleus from VAP. This problem naturally disappears when we consider the complex HF transformation.

To minimize the projected energy, one may need to evaluate the gradient of the energy, as has been done in the VAMPIR method. However, in our calculations, we realized that with the time-odd mean field, it is much more difficult to obtain a converged VAP energy. We expect this problem might be solved by calculating the Hessian matrix (i.e., the second-order partial derivatives) of the projected energy. Fortunately, our newly developed technique [6] opens the possibility of evaluating such complicated Hessian matrix. Indeed, with the Hessian matrix, our VAP calculation converges more stably.

The paper is organized as follows. Section II provides a general introduction into the VAP. Section III is devoted to the VAP calculations for some *sd*-shell nuclei. A brief summary and outlook is presented in Sec. IV.

II. THE VAP METHOD

One can start from a randomly chosen HFB vacuum state $|\Phi_0\rangle$. $|\Phi_0\rangle$ is assumed to be normalized. The corresponding quasiparticle operators for $|\Phi_0\rangle$ are denoted by $\beta_{0,\mu}^\dagger$ and $\beta_{0,\mu}$. Using the Thouless theorem [7], one can change $|\Phi_0\rangle$ to a new HFB vacuum state $|\Phi\rangle$ (with single quasiparticle operators denoted by $\beta_\mu^\dagger$ and β_μ). Namely,

$$|\Phi\rangle = \mathcal{N} e^{\frac{1}{2}\sum_{\mu\nu} d_{\mu\nu}\beta_{0,\mu}^\dagger \beta_{0,\nu}^\dagger}|\Phi_0\rangle = \mathcal{N} e^{\frac{1}{2}\sum_{\mu\nu} d_{\mu\nu}A_{\mu\nu}^\dagger}|\Phi_0\rangle, \quad (1)$$

where we define the particle pair operator,

$$A_{\mu\nu}^\dagger = \beta_{0,\mu}^\dagger \beta_{0,\nu}^\dagger, \quad (2)$$

$$A_{\mu\nu} = (\beta_{0,\mu}^\dagger \beta_{0,\nu}^\dagger)^\dagger = \beta_{0,\nu} \beta_{0,\mu}, \quad (3)$$

---
*tuya_sy@126.com
†zcgao@ciae.ac.cn

for convenience. $\mathcal{N}$ is the normalization factor so that $\langle\Phi|\Phi\rangle = 1$. d is a skew symmetric matrix, whose matrix elements are taken as the variational parameters determining $|\Phi\rangle$. Here, we assume $d_{\mu\nu}$ to be a complex number, i.e.,

$$d_{\mu\nu} = x_{\mu\nu} + iy_{\mu\nu}, \qquad (4)$$

where $x_{\mu\nu}$ and $y_{\mu\nu}$ are real numbers.

Projecting $|\Phi\rangle$ onto good particle numbers and good spin J, one gets the projected states $P^N P^Z P^J_{MK}|\Phi\rangle$. Here, P^N, P^Z, and P^J_{MK} are projection operators for the neutron number, the proton number, and the spin, respectively. The trial nuclear wave function can be written as the superposition of the projected states,

$$|\Psi_{J,M}\rangle = \sum_K f_K P^N P^Z P^J_{MK}|\Phi\rangle = \sum_K f_K P^S_{MK}|\Phi\rangle, \quad (5)$$

where we define $P^N P^Z P^J_{K'K} \equiv P^S_{K'K}$ for convenience. The corresponding projected energy then can be expressed as

$$E_J = \frac{\langle\Psi_{J,M}|\hat{H}|\Psi_{J,M}\rangle}{\langle\Psi_{J,M}|\Psi_{J,M}\rangle} = \frac{\sum_{K'K} f_{K'}^* f_K H_{K'K}}{\sum_{K'K} f_{K'}^* f_K N_{K'K}}, \qquad (6)$$

where

$$H_{K'K} = \langle\Phi|\hat{H} P^S_{K'K}|\Phi\rangle, \qquad (7)$$

$$N_{K'K} = \langle\Phi|P^S_{K'K}|\Phi\rangle. \qquad (8)$$

Actually, E_J and the corresponding f_K coefficients are obtained by solving the Hill-Wheeler (HW) equation

$$\sum_K (H_{K'K} - E_J N_{K'K}) f_K = 0. \qquad (9)$$

The f_K coefficients also satisfy the normalization condition

$$\langle\Psi_{J,M}|\Psi_{J,M}\rangle = \sum_{K'K} f_{K'}^* f_K N_{K'K} = 1. \qquad (10)$$

Clearly, E_J and f_K coefficients are functions of the d matrix. This treatment is different from the VAMPIR, where f_K are taken as independent parameters.

One may expect to find a proper d matrix so that E_J becomes a minimum. This can be done through the variation-after-projection (VAP) strategy, where the gradient of E_J has to be evaluated.

First, we do the partial derivatives with respect to $x_{\mu\nu}$ on both sides of Eqs. (9) and (10), and get a set of linear equations,

$$\frac{\partial E_J}{\partial x_{\mu\nu}} \sum_K N_{K'K} f_K - \sum_K \frac{\partial f_K}{\partial x_{\mu\nu}} (H_{K'K} - E_J N_{K'K})$$

$$= \sum_K \left(\frac{\partial H_{K'K}}{\partial x_{\mu\nu}} - E_J \frac{\partial N_{K'K}}{\partial x_{\mu\nu}} \right) f_K, \qquad (11)$$

$$\sum_K \left(f_{K'}^* \frac{\partial f_K}{\partial x_{\mu\nu}} + \frac{\partial f_{K'}^*}{\partial x_{\mu\nu}} f_K \right) N_{K'K}$$

$$= -\sum_K f_{K'}^* f_K \left(\frac{\partial N_{K'K}}{\partial x_{\mu\nu}} \right), \qquad (12)$$

where $\frac{\partial H_{K'K}}{\partial x_{\mu\nu}}$ and $\frac{\partial N_{K'K}}{\partial x_{\mu\nu}}$ can be expressed as (see more details in the Appendices)

$$\frac{\partial H_{K'K}}{\partial x_{\mu\nu}} = \langle\Phi|\hat{H} P^S_{K'K} A^\dagger_{\mu\nu}|\Phi\rangle + \langle\Phi|A_{\mu\nu}\hat{H} P^S_{K'K}|\Phi\rangle$$

$$- 2H_{K'K}\text{Re}\langle\Phi|A^\dagger_{\mu\nu}|\Phi\rangle, \qquad (13)$$

$$\frac{\partial N_{K'K}}{\partial x_{\mu\nu}} = \langle\Phi|P^S_{K'K} A^\dagger_{\mu\nu}|\Phi\rangle + \langle\Phi|A_{\mu\nu} P^S_{K'K}|\Phi\rangle$$

$$- 2N_{K'K}\text{Re}\langle\Phi|A^\dagger_{\mu\nu}|\Phi\rangle. \qquad (14)$$

The matrix elements in the right-hand sides of Eqs. (13) and (14) can be numerically calculated using our newly developed techniques [6]. Solving Eqs. (11) and (12), one can obtain $\frac{\partial E_J}{\partial x_{\mu\nu}}$ and $\frac{\partial f_K}{\partial x_{\mu\nu}}$.

For the partial derivatives $\frac{\partial E_J}{\partial y_{\mu\nu}}$ and $\frac{\partial f_K}{\partial y_{\mu\nu}}$, there exist the same linear equations as Eqs. (11) and (12) but $x_{\mu\nu}$ should be replaced by $y_{\mu\nu}$. In this case, $\frac{\partial H_{K'K}}{\partial y_{\mu\nu}}$ and $\frac{\partial N_{K'K}}{\partial y_{\mu\nu}}$ can be written as

$$\frac{\partial H_{K'K}}{\partial y_{\mu\nu}} = i(\langle\Phi|\hat{H} P^S_{K'K} A^\dagger_{\mu\nu}|\Phi\rangle - \langle\Phi|A_{\mu\nu}\hat{H} P^S_{K'K}|\Phi\rangle)$$

$$- 2i H_{K'K}\text{Im}\langle\Phi|A^\dagger_{\mu\nu}|\Phi\rangle, \qquad (15)$$

$$\frac{\partial N_{K'K}}{\partial y_{\mu\nu}} = i\left(\langle\Phi|P^S_{K'K} A^\dagger_{\mu\nu}|\Phi\rangle - \langle\Phi|A_{\mu\nu} P^S_{K'K}|\Phi\rangle\right)$$

$$- 2i N_{K'K}\text{Im}\langle\Phi|A^\dagger_{\mu\nu}|\Phi\rangle. \qquad (16)$$

On the other side, one can directly derive the gradient of the energy E_J from Eq. (6):

$$\frac{\partial E_J}{\partial x_{\mu\nu}} = \frac{\sum_{K'K}\left[f_{K'}^* f_K \left(\frac{\partial H_{K'K}}{\partial x_{\mu\nu}} - E_J \frac{\partial N_{K'K}}{\partial x_{\mu\nu}} \right) \right]}{\langle\Psi_{J,M}|\Psi_{J,M}\rangle}$$

$$+ \frac{\sum_{K'K}\left[\left(\frac{\partial f_{K'}^*}{\partial x_{\mu\nu}} f_K + f_{K'}^* \frac{\partial f_K}{\partial x_{\mu\nu}} \right)(H_{K'K} - E_J N_{K'K}) \right]}{\langle\Psi_{J,M}|\Psi_{J,M}\rangle}.$$

$$(17)$$

The second term in the right-hand side of above equation vanishes due to the HW equation, so we have

$$\frac{\partial E_J}{\partial x_{\mu\nu}} = \frac{\sum_{K'K}\left[f_{K'}^* f_K \left(\frac{\partial H_{K'K}}{\partial x_{\mu\nu}} - E_J \frac{\partial N_{K'K}}{\partial x_{\mu\nu}} \right) \right]}{\langle\Psi_{J,M}|\Psi_{J,M}\rangle}. \qquad (18)$$

The above equation also holds if $x_{\mu\nu}$ is replaced by $y_{\mu\nu}$. Our numerical calculations have confirmed that the gradients of E_J from Eq. (18) and from Eqs. (11) and (12) are indeed identical. The quantities of $\frac{\partial f_K}{\partial x_{\mu\nu}}$ and $\frac{\partial f_K}{\partial y_{\mu\nu}}$ obtained from Eqs. (11) and (12) look useless, and one might prefer to use Eq. (18). However, $\frac{\partial f_K}{\partial x_{\mu\nu}}$ and $\frac{\partial f_K}{\partial y_{\mu\nu}}$ are required if one wants to calculate the second-order partial derivatives of E_J, i.e., the Hessian matrix.

In the numerical optimization, Hessian matrix plays important roles. First it can be used to test if a critical point with zero gradient is a local minimum, local maximum, or a saddle point. In the present work, we try to search for the energy minimum, so the Hessian matrix at the minimum should be positive or semipositive definite. It is known that an isolated minimum should have positive definite Hessian matrix. However, this is

not our case because the VAP energy minimum is not isolated. One can imagine that if a state $|\Phi\rangle$ is at the energy minimum, then the rotated state $|\Phi'\rangle = \hat{R}(\Omega)|\Phi\rangle$ corresponds to the same energy. Clearly, $|\Phi\rangle$ and $|\Phi'\rangle$ have different d matrices. Thus our Hessian matrix should be semipositive definite.

In quasi-Newton's method, the minimum is always assumed to be isolated. Correspondingly, the approximated Hessian matrix is imposed to be positive definite at the minimum. We have applied the Broyden–Fletcher–Goldfarb–Shanno (BFGS) algorithm to our previous calculations [5], and it does work in the case where the mean field has time reversal symmetry. However in the present case, the time reversal symmetry is broken, the BFGS method converges very slowly or sometimes even does not converge at all. Under this situation, we are forced to come back to the Newton's method in which the Hessian matrix needs to be exactly calculated.

The evaluation of the Hessian matrix is more complicated. The second partial derivative of E_J with respect to $x_{\mu\nu}$ and $x_{\mu'\nu'}$ can be further deduced based on Eq. (18):

$$
\begin{aligned}
\frac{\partial^2 E_J}{\partial x_{\mu\nu} \partial x_{\mu'\nu'}} =& \sum_{K'K} f_{K'}^* f_K \left(\frac{\partial^2 H_{K'K}}{\partial x_{\mu\nu} \partial x_{\mu'\nu'}} - E_J \frac{\partial^2 N_{K'K}}{\partial x_{\mu\nu} \partial x_{\mu'\nu'}} \right) \\
& - \sum_{K'K} f_{K'}^* f_K \left(\frac{\partial E_J}{\partial x_{\mu\nu}} \frac{\partial N_{K'K}}{\partial x_{\mu'\nu'}} + \frac{\partial E_J}{\partial x_{\mu'\nu'}} \frac{\partial N_{K'K}}{\partial x_{\mu\nu}} \right) \\
& - \sum_{K'K} \left(\frac{\partial f_{K'}^*}{\partial x_{\mu\nu}} \frac{\partial f_K}{\partial x_{\mu'\nu'}} + \frac{\partial f_{K'}^*}{\partial x_{\mu'\nu'}} \frac{\partial f_K}{\partial x_{\mu\nu}} \right) \\
& \times (H_{K'K} - E_J N_{K'K}).
\end{aligned}
\tag{19}
$$

Notice that we have applied Eq. (11) in obtaining Eq. (19). The matrix elements $\frac{\partial^2 H_{K'K}}{\partial x_{\mu\nu} \partial x_{\mu'\nu'}}$ and $\frac{\partial^2 N_{K'K}}{\partial x_{\mu\nu} \partial x_{\mu'\nu'}}$ in Eq. (19) can be numerically evaluated using the explicit expressions in the Appendices. One also needs to evaluate $\frac{\partial^2 E_J}{\partial x_{\mu\nu} \partial y_{\mu'\nu'}}$ and $\frac{\partial^2 E_J}{\partial y_{\mu\nu} \partial y_{\mu'\nu'}}$ which forms are the same as Eq. (19) but $x_{\mu\nu}$ (or $x_{\mu'\nu'}$) should be replaced by $y_{\mu\nu}$ (or $y_{\mu'\nu'}$).

Once we have E_J, the gradient and the Hessian of E_J, the minimization of E_J becomes a optimization problem which can be solved using the trust region algorithm [8].

III. THE NUMERICAL CALCULATIONS

In the present work, we reduce $|\Phi_0\rangle$ and $|\Phi\rangle$ to be Hartree-Fock (HF) Slater determinants (SD). So the particle number projection can be omitted. This saves much computational time because we only perform the spin projection.

Let us first establish the initial $|\Phi_0\rangle$ SD, which is the starting point in our VAP. The spherical single particle basis in a M-dimensional model space is denoted by $|i\rangle \equiv |Nljm\rangle$. The corresponding creation and annihilation operators are denoted by $c_i^\dagger$ and c_i, respectively.

Following the notations of the textbook by Ring and Schuck [7], the HFB transformation is written as

$$
\begin{pmatrix} c \\ c^\dagger \end{pmatrix} = \begin{pmatrix} U_0 & V_0^* \\ V_0 & U_0^* \end{pmatrix} \begin{pmatrix} \beta_0 \\ \beta_0^\dagger \end{pmatrix} = \begin{pmatrix} U & V^* \\ V & U^* \end{pmatrix} \begin{pmatrix} \beta \\ \beta^\dagger \end{pmatrix}.
\tag{20}
$$

Here, we do not mix the neutron states with the proton states in the HFB transformation. The simplest HFB transformation

is $U = I$ and $V = 0$. I is the unit matrix. The corresponding vacuum is the true vacuum $|0\rangle$ with $c_i|0\rangle = 0$. Based on such trivial HFB transformation, one can exchange the first $n(\leqslant M)$ columns of U and V. The resulting vacuum for the new U, V becomes $|\Phi_{00}\rangle \equiv \prod_{i=1}^n c_i^\dagger |0\rangle$, i.e., the SD with the first n orbits occupied. The corresponding creation operator becomes

$$
\beta_{00,\mu}^\dagger = \begin{cases} c_\mu^\dagger, & \text{for } \mu > n \\ c_\mu, & \text{for } \mu \leqslant n \end{cases}.
\tag{21}
$$

Now, $|\Phi_0\rangle$ can be obtained from $|\Phi_{00}\rangle$ through the Thouless formula,

$$
|\Phi_0\rangle = \mathcal{N}_0 e^{\frac{1}{2} \sum_{\mu\nu} d_{0,\mu\nu} \beta_{00,\mu}^\dagger \beta_{00,\nu}^\dagger} |\Phi_{00}\rangle.
\tag{22}
$$

To keep the particle number a good quantum number, the nonzero parameters are those whose $\beta_{00,\mu}^\dagger \beta_{00,\nu}^\dagger$ pairs do not change the particle number. In other words, according to Eq. (21), the indexes μ and ν in $d_{0,\mu\nu}$ should satisfy that $\mu > n$ and $\nu \leqslant n$, or $\mu \leqslant n$ and $\nu > n$. This constraint is also valid for the d matrix in Eq. (1). Considering the skew symmetry of the d matrix, one can easily count the number of independent $d_{\mu\nu}$ matrix elements, denoted by D_{VAP}. More explicitly,

$$
D_{\text{VAP}} = N(M_N - N) + Z(M_Z - Z),
\tag{23}
$$

where N and Z are valent neutrons and protons, respectively. M_N and M_Z are the dimensions of the model spaces for neutron and proton. Notice that for a given nucleus, D_{VAP} is independent of the spin. For instance, in the sd shell model space, $D_{\text{VAP}} = 64$ for all spins in ^{24}Mg. Since $d_{\mu\nu}$ is complex, the number of the independent VAP parameters is actually $2D_{\text{VAP}}$. So, the $|\Phi_0\rangle$ can be randomly established by randomly chosen the nonzero $d_{0,\mu\nu}$ parameters in Eq. (22).

We start the VAP calculation with $|\Phi\rangle = |\Phi_0\rangle$ by setting d in Eq. (1) to zero. The iteration terminates when the gradient of the E_J becomes less than 0.1 keV. This is a very strict condition so that the converged energy almost reaches the exact minimum. Moreover, to confirm the lowest minimum, we perform the VAP calculations using different initial $|\Phi_0\rangle$ states. All the final converged energies are collected, and one may find that the lowest minimum appears repeatedly. We take the lowest converged energy (denoted by E_{VAP}) as our final VAP result.

Because the time reversal symmetry is broken in the HF mean field, the present VAP can be extended to the calculations for the odd-spin states in even-even nuclei and all the yrast states in odd-A and odd-odd nuclei. In the practical VAP calculations, we adopted the USDB Hamiltonian [9]. As testing examples, the yrast states in ^{24}Mg, ^{25}Mg, ^{26}Mg, and ^{26}Al have been calculated. These nuclei represent the even-even, odd-A, and odd-odd ones, respectively. All the calculations are performed using the same code. The VAP energies as well as the shell model ones are shown in Fig. 1. We should remind that in calculating the high-spin states, there is a new difficulty that the norm of the high-K projected states are usually very tiny. This may lead to large calculation errors in the evaluations of the involved VAP matrix elements. To avoid this problem, we actually omitted those projected components with $K \geqslant 5$.
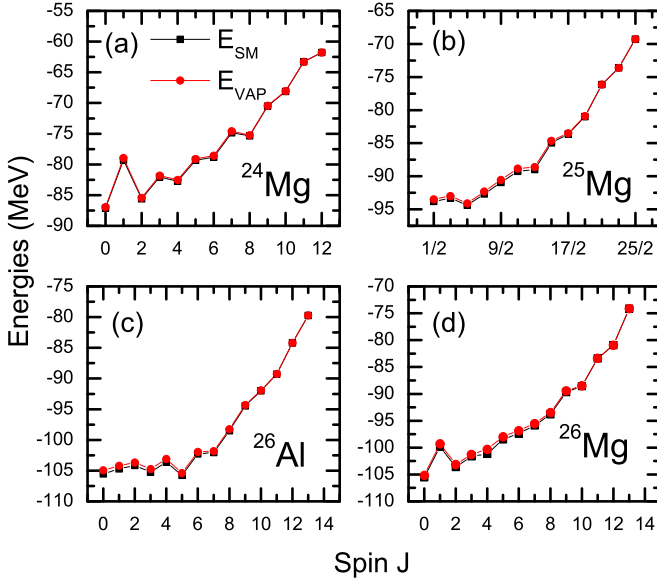
FIG. 1. Calculated VAP energies E_{VAP} and the shell model energies E_{SM}, with the USDB interaction along the yrast line for (a) ^{24}Mg, (b) ^{25}Mg, (c) ^{26}Al, and (d) ^{26}Mg.

One can clearly see in Fig. 1 that the VAP results are very close to the shell model ones which are obtained from the NUSHELLX code [10]. However, we used only a single slater determinant and only did the spin projection. The present results clearly show that the spin projection is very important in achieving a good approximation to the full shell model.

To show the energy difference between VAP and SM more clearly, we plot in Fig. 2 the corresponding $E_{\mathrm{VAP}} - E_{\mathrm{SM}}$ energies. Up to the median spin region ($J \leqslant 6$), $E_{\mathrm{VAP}} - E_{\mathrm{SM}}$ ranges from 200 keV to 600 keV. With spin increasing higher, $E_{\mathrm{VAP}} - E_{\mathrm{SM}}$ decreases, and even becomes zero at the highest
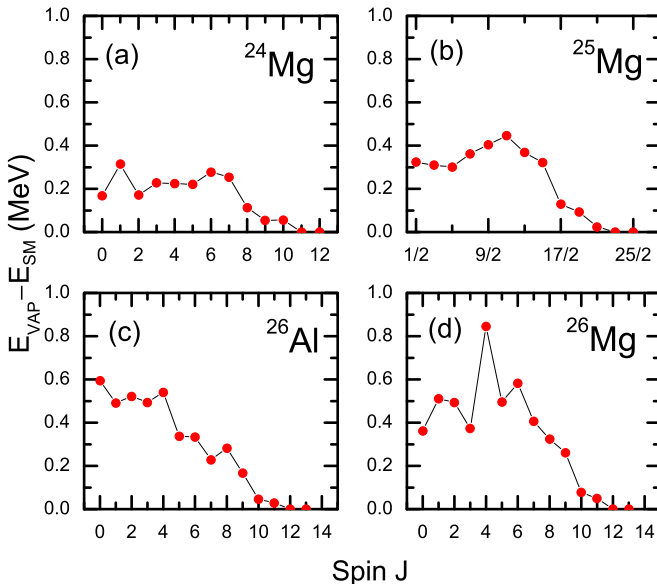
FIG. 2. The energy differences between the shell model energies E_{SM}, and the present VAP energies E_{VAP}.
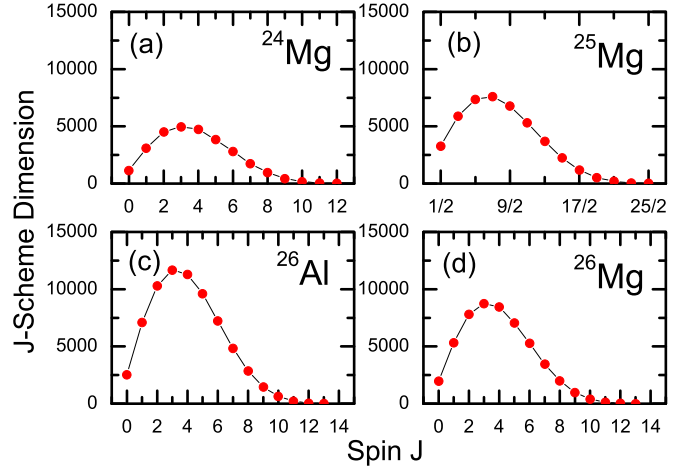
FIG. 3. The J-scheme shell model dimension as a function of the spin, J, for the calculated nuclei in sd model space.

two spins. This behavior of $E_{\mathrm{VAP}} - E_{\mathrm{SM}}$ may be related to the shell model configuration space. The shell model dimensions as functions of the spin J are shown in Fig. 3. It is seen that the J-scheme shell model dimension also decreases since $J > 4$. Such similar trends indicate that the VAP wave function is more close to shell model wave function if the configuration space is small. However for $J \leqslant 4$, the situation looks different. The shell model dimension decreases with spin decreasing. But $E_{\mathrm{VAP}} - E_{\mathrm{SM}}$ roughly remains unchanged. One may consider that the ground state is a superfluidity state, and a single slater determinant should not fully account for the pairing effect. This might be a reason why $E_{\mathrm{VAP}} - E_{\mathrm{SM}}$ does not decrease with shell model configuration space shrinking.

However, in our previous VAP calculations [5], we indeed took the HFB vacuum state and performed the spin (J), the isospin (T), and the mass number (A) projections. The VAP with JTA projection should have properly accounted for the pairing effect. But in that VAP-JTA calculations, we imposed the time reversal symmetry, real d matrix, and the symmetry of $e^{i\pi \hat{J}_z}$ (rotation around z axis by π angle). Thus this VAP-JTA can only be applied to the even spins in even-even nuclei. Under the above constraints, the number of the VAP-JTA parameters is 42 for all calculated sd even-even nuclei. The energy differences $E_{\mathrm{JTA}} - E_{\mathrm{SM}}$ at $J = 0$ are compared with the present $E_{\mathrm{VAP}} - E_{\mathrm{SM}}$ in Fig. 4. It is interesting that most of the present VAP energies are even lower than the VAP-JTA energies despite VAP-JTA takes the HFB mean field and recovers all the quantum numbers. However, the present HF mean field breaks the symmetries of the time reversal and $e^{i\pi \hat{J}_z}$, and allows the d matrix to be complex. This leads the number of the parameters, $2D_{\mathrm{VAP}}$, much larger than that of VAP-JTA. Thus the present VAP wave function might have even larger overlap with the shell model wave function. However, if we impose the same constraints as the VAP-JTA to the present HF mean field, this may considerably reduce the number of VAP parameters. Consequently, the corresponding VAP energies E_{PHF}, which have been calculated in Ref. [5] and also shown in Fig. 4 here, are higher than both E_{JTA} and E_{VAP}, but yet within 1.5 MeV relative to the shell model ones.
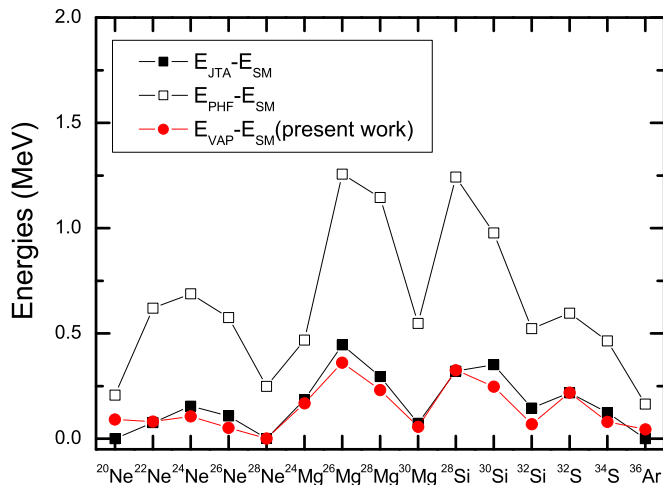
FIG. 4. The relative energies of E_{VAP} (present), E_{JTA} [5], and E_{PHF} [5] to the SM energies E_{SM} for the ground states of even-even sd nuclei.

To check if the Hessian is semipositive definite or not at the minimum, we calculated the eigenvalues, λ_i, of the Hessian and show them in Fig. 5. For the initial HF vacuum $|\Phi_0\rangle$, the eigenvalues are both positive and negative. This means the Hessian matrix is indefinite. When the VAP iteration converges, it is clearly shown in Fig. 5 that $\lambda_i \geqslant 0$ for all i. Moreover, one can see that almost half of the eigenvalues are very close to zero. This confirms the Hessian matrix is semipositive definite at the energy minimum.

The present VAP wave function is actually a projected Slater determinant, the form of which is shown in Eq. (5), where the particle number projection operators, P^N and P^Z, should be removed and $|\Phi\rangle$ can be replaced by a Slater determinant. It looks that this simple form of nuclear wave function can be easily applied to heavier nuclei in the practical calculations.
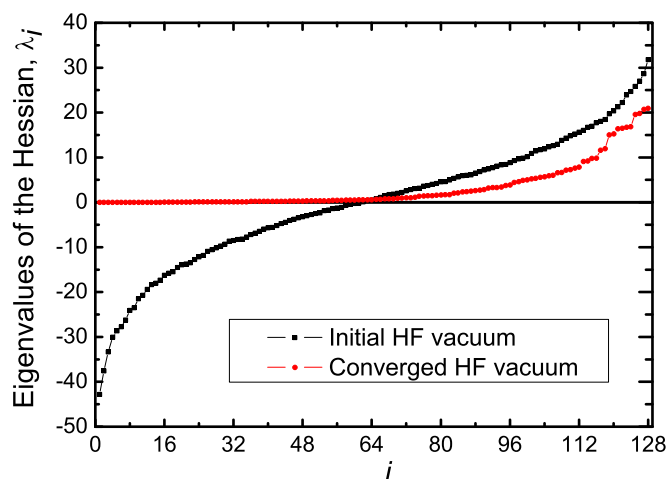
FIG. 5. Eigenvalues of the Hessian matrix of the projected energy for the ground state of ^{24}Mg. The black filled rectangles show the ones at an initial HF vacuum $|\Phi_0\rangle$. The red filled dots show the ones at the converged HF vacuum. The total number of the independent VAP parameters is $2D_{\mathrm{VAP}} = 128$.
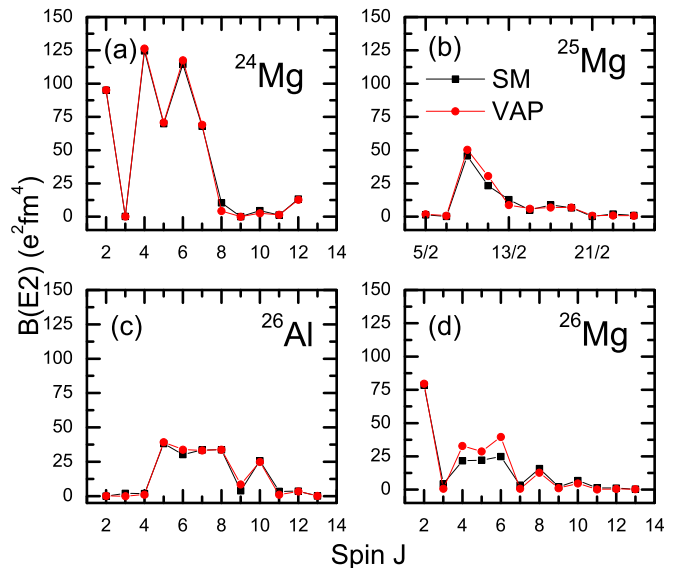
FIG. 6. Calculated $B(E2 : I \rightarrow I - 2)$ values from VAP (red filled circles) and SM (black filled squares) with the wave functions corresponding to Fig. 1. The effective charges are taken as $e_n = 0.5e, e_p = 1.5e$, and the oscillator value $\hbar\omega = 45A^{-1/3} - 25A^{-2/3}$ MeV.

Using the VAP wave functions, one can easily calculate other observables. As a preliminary test, we calculated the $B(E2 : I \rightarrow I - 2)$ values with the wave functions corresponding to the energies in Fig. 1. As shown in Fig. 6, the $B(E2)$ values from VAP are generally close the ones from SM [10]. This shows that the present VAP wave functions are also good approximations to the exact shell model ones.

IV. SUMMARY AND OUTLOOK

Based on the time-odd HF slater determinant, we have successfully implemented the VAP calculations using our newly developed techniques. This VAP now can be reliably applied to the yrast states in all kinds of nuclei. In the present VAP, we have successfully calculated the Hessian matrix as well as the gradient of the projected energy which makes the VAP calculation converges more stably. Although only the spin projection is involved, the present VAP still has achieved a very good approximation to the shell model and even better than our previous VAP-JTA results [5]. This further confirms the conclusion made in our previous work [5] that the spin projection plays a key role.

One may expect that the present VAP can be further developed by including more projected SDs in the VAP wave function. This will not only improve the present results, but also make it possible to extend the VAP calculations to the nonyrast states, as have done in the excited VAMPIR. But in the latter, the HFB vacua are practically time-even and axially symmetric so that the computational time can be considerable reduced. In our case, we plan to take nonaxial time-odd HF SDs as adopted in the present calculations. Such work is under working, and we hope the new VAP results for nonyrast states will come out in the near future.

On the other hand, one may expect to release the constraints of the VAP-JTA and take the most general HFB mean field to do the VAP-JTA calculation, which is similar to the the GCV calculation [4]. This should have even better results, but it is also very much time consuming due to the seven-dimensional integration for the JTA projection. Therefore, this may be very hard to apply such VAP calculation to the heaver nuclear region. Thus we do not plan to go further along this line for the moment.

APPENDIX A: GRADIENT OF THE PROJECTED MATRIX ELEMENTS

We define

$$|\Theta\rangle = e^{\frac{1}{2}\sum_{\mu\nu} d_{\mu\nu} A_{\mu\nu}^\dagger}|\Phi_0\rangle, \tag{A1}$$

then the normalized HFB vacuum, $|\Phi\rangle$, can be written as

$$|\Phi\rangle = \frac{|\Theta\rangle}{\sqrt{\langle\Theta|\Theta\rangle}}. \tag{A2}$$

So, the projected matrix element in Eq. (7) becomes

$$H_{K'K} = \frac{\langle\Theta|\hat{H}P_{K'K}^S|\Theta\rangle}{\langle\Theta|\Theta\rangle}. \tag{A3}$$

Using the identities

$$\frac{\partial|\Theta\rangle}{\partial x_{\mu\nu}} = \frac{\partial d_{\mu\nu}}{\partial x_{\mu\nu}}\frac{\partial|\Theta\rangle}{\partial d_{\mu\nu}} = A_{\mu\nu}^\dagger|\Theta\rangle, \tag{A4}$$

$$\frac{\partial\langle\Theta|}{\partial x_{\mu\nu}} = \frac{\partial d_{\mu\nu}^*}{\partial x_{\mu\nu}}\frac{\partial\langle\Theta|}{\partial d_{\mu\nu}^*} = \langle\Theta|A_{\mu\nu}, \tag{A5}$$

one can deduce that

$$\begin{aligned}\frac{\partial H_{K'K}}{\partial x_{\mu\nu}} &= \frac{1}{\langle\Theta|\Theta\rangle}\frac{\partial\langle\Theta|\hat{H}P_{K'K}^S|\Theta\rangle}{\partial x_{\mu\nu}} - \frac{H_{K'K}}{\langle\Theta|\Theta\rangle}\frac{\partial\langle\Theta|\Theta\rangle}{\partial x_{\mu\nu}}\\ &= \frac{\langle\Theta|\hat{H}P_{K'K}^S A_{\mu\nu}^\dagger|\Theta\rangle + \langle\Theta|A_{\mu\nu}\hat{H}P_{K'K}^S|\Theta\rangle}{\langle\Theta|\Theta\rangle}\\ &\quad - H_{K'K}\frac{\langle\Theta|A_{\mu\nu}|\Theta\rangle + \langle\Theta|A_{\mu\nu}^\dagger|\Theta\rangle}{\langle\Theta|\Theta\rangle}\\ &= \langle\Phi|\hat{H}P_{K'K}^S A_{\mu\nu}^\dagger|\Phi\rangle + \langle\Phi|A_{\mu\nu}\hat{H}P_{K'K}^S|\Phi\rangle\\ &\quad - H_{K'K}[\langle\Phi|A_{\mu\nu}|\Phi\rangle + \langle\Phi|A_{\mu\nu}^\dagger|\Phi\rangle]. \end{aligned} \tag{A6}$$

$\frac{\partial N_{K'K}}{\partial x_{\mu\nu}}$ can also be obtained by setting $\hat{H} = 1$ in Eq. (A6). Similarly, using

$$\frac{\partial|\Theta\rangle}{\partial y_{\mu\nu}} = \frac{\partial d_{\mu\nu}}{\partial y_{\mu\nu}}\frac{\partial|\Theta\rangle}{\partial d_{\mu\nu}} = iA_{\mu\nu}^\dagger|\Theta\rangle, \tag{A7}$$

$$\frac{\partial\langle\Theta|}{\partial y_{\mu\nu}} = \frac{\partial d_{\mu\nu}^*}{\partial y_{\mu\nu}}\frac{\partial\langle\Theta|}{\partial d_{\mu\nu}^*} = -i\langle\Theta|A_{\mu\nu}, \tag{A8}$$

one can also get Eqs. (15) and (16).

APPENDIX B: HESSIAN OF THE PROJECTED MATRIX ELEMENTS

Based on the expressions of $\frac{\partial H_{K'K}}{\partial x_{\mu\nu}}$, one can further deduce the Hessian of $H_{K'K}$. Here, we only present the final expressions of the Hessian matrix elements:

$$\begin{aligned}&\frac{\partial^2 H_{K'K}}{\partial x_{\mu\nu}\partial x_{\mu'\nu'}}\\ &= \langle\Phi|\hat{H}P_{K'K}^S A_{\mu\nu}^\dagger A_{\mu'\nu'}^\dagger|\Phi\rangle + \langle\Phi|A_{\mu\nu}\hat{H}P_{K'K}^S A_{\mu'\nu'}^\dagger|\Phi\rangle\\ &\quad + \langle\Phi|A_{\mu'\nu'}\hat{H}P_{K'K}^S A_{\mu\nu}^\dagger|\Phi\rangle + \langle\Phi|A_{\mu\nu}A_{\mu'\nu'}\hat{H}P_{K'K}^S|\Phi\rangle\\ &\quad - 2\frac{\partial H_{K'K}}{\partial x_{\mu\nu}}\mathrm{Re}\langle\Phi|A_{\mu'\nu'}^\dagger|\Phi\rangle - 2\frac{\partial H_{K'K}}{\partial x_{\mu'\nu'}}\mathrm{Re}\langle\Phi|A_{\mu\nu}^\dagger|\Phi\rangle\\ &\quad - 2H_{K'K}\mathrm{Re}[\langle\Phi|A_{\mu\nu}^\dagger A_{\mu'\nu'}^\dagger|\Phi\rangle + \langle\Phi|A_{\mu\nu}A_{\mu'\nu'}^\dagger|\Phi\rangle],\end{aligned} \tag{B1}$$

$$\begin{aligned}&\frac{\partial^2 H_{K'K}}{\partial x_{\mu\nu}\partial y_{\mu'\nu'}}\\ &= i\langle\Phi|\hat{H}P_{K'K}^S A_{\mu\nu}^\dagger A_{\mu'\nu'}^\dagger|\Phi\rangle + i\langle\Phi|A_{\mu\nu}\hat{H}P_{K'K}^S A_{\mu'\nu'}^\dagger|\Phi\rangle\\ &\quad - i\langle\Phi|A_{\mu'\nu'}\hat{H}P_{K'K}^S A_{\mu\nu}^\dagger|\Phi\rangle - i\langle\Phi|A_{\mu\nu}A_{\mu'\nu'}\hat{H}P_{K'K}^S|\Phi\rangle\\ &\quad + 2\frac{\partial H_{K'K}}{\partial x_{\mu\nu}}\mathrm{Im}\langle\Phi|A_{\mu'\nu'}^\dagger|\Phi\rangle - 2\frac{\partial H_{K'K}}{\partial y_{\mu'\nu'}}\mathrm{Re}\langle\Phi|A_{\mu\nu}^\dagger|\Phi\rangle\\ &\quad + 2H_{K'K}\mathrm{Im}[\langle\Phi|A_{\mu\nu}^\dagger A_{\mu'\nu'}^\dagger|\Phi\rangle + \langle\Phi|A_{\mu\nu}A_{\mu'\nu'}^\dagger|\Phi\rangle],\end{aligned} \tag{B2}$$

$$\begin{aligned}&\frac{\partial^2 H_{K'K}}{\partial y_{\mu\nu}\partial y_{\mu'\nu'}}\\ &= -\langle\Phi|\hat{H}P_{K'K}^S A_{\mu\nu}^\dagger A_{\mu'\nu'}^\dagger|\Phi\rangle + \langle\Phi|A_{\mu\nu}\hat{H}P_{K'K}^S A_{\mu'\nu'}^\dagger|\Phi\rangle\\ &\quad + \langle\Phi|A_{\mu'\nu'}\hat{H}P_{K'K}^S A_{\mu\nu}^\dagger|\Phi\rangle - \langle\Phi|A_{\mu\nu}A_{\mu'\nu'}\hat{H}P_{K'K}^S|\Phi\rangle\\ &\quad + 2\frac{\partial H_{K'K}}{\partial y_{\mu\nu}}\mathrm{Im}\langle\Phi|A_{\mu'\nu'}^\dagger|\Phi\rangle + 2\frac{\partial H_{K'K}}{\partial y_{\mu'\nu'}}\mathrm{Im}\langle\Phi|A_{\mu\nu}^\dagger|\Phi\rangle\\ &\quad + 2H_{K'K}\mathrm{Re}[\langle\Phi|A_{\mu\nu}^\dagger A_{\mu'\nu'}^\dagger|\Phi\rangle - \langle\Phi|A_{\mu\nu}A_{\mu'\nu'}^\dagger|\Phi\rangle].\end{aligned} \tag{B3}$$

The Hessian of $N_{K'K}$ can be directly obtained from Eqs. (B1)–(B3) by setting $\hat{H} = 1$.

[1] S. E. Koonin, D. J. Dean, and K. Langanke, Phys. Rep. **278**, 1 (1997).

[2] T. Otsuka, M. Honma, T. Mizusaki, N. Shimizu, and Y. Utsuno, Prog. Part. Nucl. Phys. **47**, 319 (2001).

[3] M. Horoi, B. A. Brown, and V. Zelevinsky, Phys. Rev. C **50**, R2274 (1994).

[4] K. W. Schmid, Prog. Part. Nucl. Phys. **52**, 565 (2004).

[5] Z.-C. Gao, Mihai Horoi, and Y. S. Chen, Phys. Rev. C **92**, 064310 (2015).

[6] Q.-L. Hu, Z.-C. Gao, and Y. S. Chen, Phys. Lett. B **734**, 162 (2014).

[7] P. Ring and P. Schuck, *The Nuclear Many-Body Problem* (Springer Verlag, New York/Heidelberg/Berlin, 1980).

[8] J. Norcedal and S. J. Wright, *Numerical Optimization* (Springer Verlag, New York/Berlin/Heidelberg, 2006).

[9] B. A. Brown and W. A. Richter, Phys. Rev. C **74**, 034315 (2006).

[10] B. A. Brown, W. D. M. Rae, E. McDonald, and M. Horoi, NuShellX@MSU, http://www.nscl.msu.edu/~brown/resources/resources.html; W. D. M. Rae, NUSHELLX, http://www.garsington.eclipse.co.uk/.